Instituto de Física
Universidade de São Paulo

Effect of the ^{18}O nuclear density in the nuclear potentials of the $^{18}O+^{58,60}Ni$ systems

Rossi Jr., E.S. [a]; Pereira, D. [a]; Chamon, L.C. [a]; Silva, C.P. [a]; Gasques, L.R. [a]; Lubian, J. [b]; Carlson, B.V. [c] and De Conti, C. [c]

[a] Departamento de Física Nuclear, Instituto de Física, Universidade de São Paulo
Caixa Postal 66318, 05315-970 São Paulo, SP, Brazil
[b] Instituto de Física, Universidade Federal Fluminense, Av. Litorânea,
Niterói, RJ 24210-340, Brazil
Permanent address: CEADEN, PO 6122, Havana, Cuba
[c] Departamento de Física, Instituto Tecnológico de Aeronáutica, Centro Técnico Aeroespacial, São José dos Campos, SP, Brazil

Publicação IF - 1545/2002

UNIVERSIDADE DE SÃO PAULO
Instituto de Física
Cidade Universitária
Caixa Postal 66.318
05315-970 - São Paulo - Brasil

Effect of the ^{18}O nuclear density in the nuclear potentials of the ^{18}O + ^{58,60}Ni systems.

E. S. Rossi Jr.[a], D. Pereira[a], L. C. Chamon[a], C. P. Silva[a], M. A. G. Alvarez[a], L. R. Gasques[a], J. Lubian[b], B. V. Carlson[c] and C. De Conti[c].

[a] *Departamento de Física Nuclear, Instituto de Física da Universidade de São Paulo, Caixa Postal 66318, 05315-970, São Paulo, SP, Brazil.*

[b] *Instituto de Física, Universidade Federal Fluminense, Av. Litoranea, Niterói, RJ, 24210-340, Brazil. Permanent address: CEADEN, PO 6122, Havana, Cuba.*

[c] *Departamento de Física, Instituto Tecnológico de Aeronáutica, Centro Técnico Aeroespacial, São José dos Campos, SP, Brazil.*

Quasi-elastic, inelastic, one- and two-neutron transfer differential cross sections have been measured for the ^{18}O + ^{58,60}Ni systems at sub-barrier energies. The corresponding bare potentials have been determined at interaction distances larger than the respective barrier radii, and the results have been compared with those previously obtained for systems involving the ^{16}O as projectile. The detected difference between the ^{18}O and ^{16}O nuclear potentials has allowed the determination of the nuclear density that corresponds to the two extra neutrons of the ^{18}O nucleus.

PACS: 24.10.Ht, 21.10.Ft, 21.10.Gv
Keywords: Heavy-ion nuclear potential. Nuclear density. Coupled-channel calculations.

1. Introduction

In this work we present quasi-elastic, inelastic, one- and two-neutron transfer differential cross sections for the ^{18}O + ^{58,60}Ni systems at sub-barrier energies. The purpose of the experiments was the determination of the corresponding nuclear potentials in an interaction region near the respective barrier radii. The method was earlier applied to several systems involving the ^{16}O nucleus as projectile [1–4]. The quasi-elastic cross section is defined as the sum of the elastic scattering with all peripheral reaction channels. No extra peripheral absorption should be expected in analysing the quasi-elastic data set, and therefore the imaginary part of the optical potential must be negligible at the surface region. Thus, the quasi-elastic data analysis unambiguously determines the real part of the interaction. The optical potential is composed of the bare and polarization potentials, the latter containing the contribution arising from nonelastic couplings. The real part of the polarization has been estimated earlier [1–3] through extensive coupled-channel calculations for the ^{16}O sub-barrier data set, and represents about 10% in comparison with the bare (nuclear) interaction. Therefore, in the ^{16}O case the experimentally extracted optical potential strengths at sub-barrier energies can be associated with the bare potential within 10% precision. In the present work, we demonstrate that the real part of the optical potential extracted from quasi-elastic data analysis for the ^{18}O + ^{58,60}Ni systems can also be associated with the bare potential within a similar precision.

In a recent work [5], an extensive systematics of optical potential strengths extracted from heavy-ion elastic scattering data analyses at low and intermediate energies was presented. The energy-dependence of the nuclear potential has been accounted for within a model based on the nonlocal nature of the interaction [5–8]. The systematics indicates that the heavy-ion potential can be described in a global way, through a double-folding shape which basically presents a simple dependence only on the densities of the partners in the collision. In the present work, by assuming this nonlocal model for the interaction and considering the detected difference between the nuclear potentials for systems involving ^{18}O and ^{16}O as projectiles, we have obtained information about the nuclear density that corresponds to the two extra neutrons of the ^{18}O nucleus.

The paper is organized as follows. In Section 2, we present the experimental results. The determination of the bare potential strengths from optical model data analyses for the ^{18}O + ^{58,60}Ni systems is described in Section 3. A brief summary of the nonlocal model, and the comparison between the present results with those for systems with ^{16}O are contained in Section 4. Section 5 is devoted to the study of the nuclear densities for the ^{16,18}O nuclei. Section 6 contains a brief summary and the main conclusions.

2. Experimental results

The measurements were made at the São Paulo 8UD Pelletron Accelerator, Brazil. The thickness of the targets was about 60 $\mu g/cm^2$. The detecting system is composed (see Fig. 1a) of nine surface barrier detectors (SBD) and three position sensitive detectors (PSD). The data acquisition has been performed through two modes: with and without coincidence of lighter particles in the SBD with heavier recoil particles in the PSD (see Fig. 1b). As the PSD have been positioned at forward angles, an electrostatic deflector has been used to decrease the number of ^{18}O nuclei elastically scattered by the nickel target that reach the detectors. The electrostatic potential between the plates of the deflector was chosen to allow the detection of the heavier recoil particles. The kinematics of the reaction provides the following expression for the mass of the lighter particle detected in the SBD:

$$A = \frac{E_{Lab}\, A_P\, sin^2(\theta_R)}{E_L\, sin^2(\theta_R + \theta_{SBD})}\,, \tag{1}$$

where E_{Lab} = bombarding energy, A_P= mass of the projectile, E_L = lighter particle energy, θ_{SBD}=angle of the SB detector, θ_R = angle of the heavier recoil particle detected in coincidence at the PSD. Fig. 2 presents a typical mass *versus* energy spectrum for the lighter particle, and also a projection of all events on the energy axis. The coincidence mode has been used only to identify the different processes (elastic, inelastic and transfer) that occur in the collision (see Fig. 2). The corresponding cross sections have been obtained by considering events in the no-coincidence mode energy spectra. This procedure is appropriate to obtain experimental cross sections without the inclusion of an efficiency of detection in the calculations, which should be included if the cross sections are calculated considering events obtained in the coincidence mode.

We define the quasi-elastic cross section as the sum over all channels with energy between the inelastic excitation of the ^{18}O 2_1^+ state and the ground-state ($E^* = 0$ MeV) two-neutron transfer, including the elastic scattering (see Fig. 2). Our experiments indicate that all reaction channels with significant cross section are included in the quasi-elastic process as defined above. Figs. 3 to 6 present the data sets obtained for several sub-barrier energies.

3. Data analysis

The determination of the bare potential has been performed by first analysing only the quasi-elastic data. In the optical model calculations, we have adopted a procedure similar to that described in the analysis of the sub-barrier data for the ^{16}O + $^{58,60,62,64}Ni$, ^{88}Sr, $^{90,92}Zr$, ^{92}Mo, ^{120}Sn, ^{138}Ba, ^{208}Pb systems [1–4]. We have adopted a Woods-Saxon shape for the optical potential, with an inner imaginary part which takes into account the rather small internal absorption from barrier penetration. The values assumed for the parameters of the imaginary part of the potential result in very small strengths at the surface region. This procedure must be adopted in the analysis because peripheral reaction channels that were not included in the quasi-elastic data present negligible cross sections. Concerning depth variations of this absorptive potential, no sensitivity in the quasi-elastic cross section predictions has been detected. The depth and diffuseness parameters of the real part of the optical potential were searched for the best data fits. For each angular distribution, we have found a family of potentials which give equivalent fits. These potentials cross (see Fig. 7) at a particular distance R_S, hereafter referred as the sensitivity radius. Therefore, the nuclear potential is determined without ambiguity at R_S from the optical model quasi-elastic data analysis.

The sensitivity radius is energy-dependent, because at sub-barrier energies it is related to the classical turning point. We have used this fact to characterize the nuclear potential in the surface region (see Fig. 8). For such large interaction distances, the shape of the potential is nearly an exponential (solid lines in Fig. 8), with a diffuseness value about 0.77 fm, and with strength values at $R = 10.5$ fm of 1.02 and 1.17 MeV for the ^{18}O + $^{58,60}Ni$ systems, respectively. Considering energy-independent nuclear potentials (Woods-Saxon shape) with such characteristics, good predictions for the quasi-elastic cross sections are obtained (dashed lines in Fig. 3).

We have also performed quite complete coupled-channel (CC) calculations using the FRESCO code [9]. In Tables 1 and 2 are presented all the channels included in the CC calculations. The inelastic couplings were treated within the vibrational model, with deformation lengths (see table 3) obtained in Refs. [2,10]. A one step cluster transfer of an $s = 0$ neutron pair was assumed for the two-neutron transfer process. Due to the large number of states for neutron transfer, most of them with unknown spectroscopic factors, we have assumed in the calculations an energy-independent average spectroscopic value for all the states, which has been searched for the best data fits. In such conditions, we have found reasonable values (≈ 0.87) for these spectroscopic factors for both systems. In the CC calculations, we have used the same bare potentials determined in the optical model quasi-elastic data analysis. Such potentials provide good descriptions (see Fig. 3 to 6) for the cross sections of all measured channels within the coupled-channel formalism. Note the very similar results obtained for the quasi-elastic cross section (see Fig.3) from the optical model and CC calculations, using the same bare potential. This means that, at sub-barrier energies, the

optical model quasi-elastic data analysis incorporates in an approximate way the main contributions of the couplings, which mostly represent loss of flux from the elastic to the peripheral reaction channels, but with conservation of the quasi-elastic cross section. This should be valid if the couplings are not too strong. Similar results have been obtained also in the case of systems with ^{16}O as the projectile [11]. Therefore, our sub-barrier data studies have indicated that two equivalent methods can be used to determine the bare potential: an optical model quasi-elastic data analysis or a full coupled-channel data analysis. An inspection of Fig. 3 indicates that the 38 MeV bombarding energy seems to be the limit in which the optical model and the coupled-channel calculations give similar predictions for the quasi-elastic cross sections. This energy is about 4 MeV below the fusion barrier for both systems. The two approaches would probably result in different data-extracted potentials if the data analyses had been realized at higher energies.

4. Comparison between potentials for systems involving the ^{16}O and ^{18}O nuclei

The elastic scattering data analyses for different systems in a very large energy range have resulted in phenomenological optical potentials with significant dependence on the bombarding energy [12]. Several theoretical models have been developed to account for this energy-dependence; one of these associates the energy-dependence with nonlocal quantum effects related to the exchange of nucleons between target and projectile [5–8]. Within this model, the bare interaction V_N is connected with the folding potential V_F through

$$V_N(R,E) \approx V_F(R)\; e^{-4v^2/c^2}\;, \tag{2}$$

where c is the speed of light and v is the local relative speed between the two nuclei,

$$v^2(R,E) = \frac{2}{\mu}\left[E - V_C(R) - V_N(R,E)\right]\;. \tag{3}$$

For the Coulomb interaction, V_C, we have used the expression for the double sharp cutoff potential [13].

The folding potential depends on the densities of the two partners in the collision

$$V_F(R) = \int \rho_1(r_1)\;\rho_2(r_2)\;u_0(\vec{R} - \vec{r_1} + \vec{r_2})\;d\vec{r_1}\;d\vec{r_2}\;. \tag{4}$$

With the aim of providing a global description of the nuclear interaction, a systematization of nuclear densities has been proposed in Ref. [5], with basis on an extensive study involving charge distributions extracted from electron scattering experiments and theoretical densities calculated through the Dirac-Hartree-Bogoliubov model. This study has indicated that the two-parameter Fermi (2pF) distribution can be adopted to describe the nuclear densities, and a useful distinction between nucleon and matter distributions has been made. The radii of the 2pF distributions are well described by

$$R_i = 1.31\;A_i^{1/3} - 0.84\;fm\;, \tag{5}$$

where A is the number of nucleons of the nucleus. The nucleon and matter densities present average diffuseness values $a_N = 0.50$ fm and $a_M = 0.56$ fm, respectively. Due to effects of the structure of the nuclei, along the table of stable nuclides the R_i and a parameters vary around the corresponding average values. However, concerning the nuclear potential, the effects of the structure of the nuclei are mostly present at the surface and mainly related only to the diffuseness parameter [5].

Within this context, an extensive systematization of optical potential strengths extracted from heavy-ion elastic scattering data analyses at low and intermediate energies was performed [5]. The experimental potential strengths have been described within 25% precision, by combining Eqs. 2 and 4 through two different and equivalent methods. In the first alternative, the double-folding potential is treated in the usual interpretation: the nucleon densities and an effective nucleon-nucleon interaction for $u_0(\vec{r})$ are adopted in Eq. 4. The standard M3Y interaction "frozen" at 10 MeV/nucleon [5,7] has been assumed for the effective nucleon-nucleon interaction. In the other alternative, the matter densities are adopted in Eq. 4, with a zero-range delta function assumed for $u_0(\vec{r})$:

$$u_0(\vec{r}) = V_0\;\delta(\vec{r})\;, \tag{6}$$

with $V_0 = -456$ MeV fm^3. This zero-range alternative is interesting because it results in approximate analytical expressions for the folding potential [5]. For example, in the surface region

$$V_F(R \geq R_1 + R_2) \approx V_0\;\rho_{01}\;\rho_{02}\;\pi a_M^2\;\mathcal{R}\;g(\tau)\;(1 + s/a_M)\;e^{-s/a_M}\;, \tag{7}$$

with $s = R - (R_1 + R_2)$, $\mathcal{R} = 2R_1R_2/(R_1 + R_2)$, $\tau = s/\mathcal{R}$. The ρ_{0i} are obtained from the normalization of the densities

$$4\pi \int_0^\infty \frac{\rho_{0i}}{1 + e^{(r-R_i)/a_M}} \, r^2 \, dr = A_i \, , \tag{8}$$

and the function g is defined by:

$$g(\tau) = \frac{1 + \tau + \tau^2\zeta/3 + a_M/\mathcal{R} + (a_M/\mathcal{R} + 1/2) \, e^{-s/a_M}}{1 + \zeta\tau} \, , \tag{9}$$

$\zeta = \mathcal{R}/(R_1 + R_2)$.

Expression 2 has accounted for the energy-dependence of experimentally extracted potential strengths for a large number of different systems in a very wide energy range [5–8]. At sub-barrier energies and for radii close to the barrier radius, Eq. 2 indicates that $V_N \approx V_F$. In order to compare potentials from different systems, we have defined a reduced quantity, V_{red}, which removes the dependence of the sub-barrier potential strengths on the radii of the nuclei,

$$V_{red} = \frac{V_N}{V_0 \, \rho_{01} \, \rho_{02} \, \mathcal{R} \, g(\tau)} \tag{10}$$

Taking into account Eqs. 7 and 10, the reduced potential should be a universal function of s

$$V_{red}(s \geq 0) \approx \pi a_M^2 \, (1 + s/a_M) \, e^{-s/a_M} \, , \tag{11}$$

with the matter diffuseness close to the average value $a_M \approx 0.56$ fm [5].

In Fig. 9, the experimental reduced potential strengths (calculated from Eq. 10) are presented for several systems involving the ^{16}O and ^{18}O nuclei, as obtained from sub-barrier data analyses. The experimental results are in agreement with the theoretical prediction, Eq. 11, but different matter diffuseness values $a_M = 0.57$ fm and 0.60 fm are found for the ^{16}O and ^{18}O sets, respectively (see Fig. 9).

5. Determination of the nuclear density for the two valence neutrons of the ^{18}O nucleus

As we have discussed in Section 4, the experimentally extracted potential strengths for systems with ^{16,18}O as projectiles are compatible with the folding potential, using densities with the shape of Fermi distributions, radii obtained from Eq. 5, and matter diffuseness values $a_M = 0.57$ fm and $a_M = 0.60$ fm. In this sense, the analysis presented in Section 4 provides information about the nuclear densities of the partners in the collision. Another form of analysing the same set of cross section data, which determines the densities in a more direct procedure than that of Section 4, has been presented in Refs. [14,15]. If the nonlocal model is assumed for the heavy-ion interaction and the density of one nucleus is known, an unfolding method can be used to extract the density of the other nucleus from data analyses. The density is obtained from a procedure similar to that used in the determination of potential strengths at the sensitivity radii. Details of the method can be found in Refs. [14,15]. Fig. 10 contains the ^{16}O and ^{18}O experimental density values at the corresponding sensitivity radii obtained from data analyses of several angular distributions for different systems. We mention that the results presented in Fig. 10 refer to the nucleon densities instead of the matter densities. We point out that data analyses for systems with different targets provide consistently similar results for the density of a same projectile. The sub-barrier data analysis gives information about the density at the surface region, while inner distances are probed through the data at intermediate energies. For example, the analysis for the ^{16}O + ^{16}O system at $E_{Lab} = 1120$ MeV has provided information (see Fig. 10) about the ^{16}O density at $r \approx 2$ fm. Eq. 2 shows that at such high energy the nonlocality reduces the nuclear potential strength by about one order of magnitude in comparison with the folding potential, and this effect is very important in obtaining a reasonable experimental value for the density.

Theoretical predictions (dashed lines in Fig. 10) from the Dirac-Hartree-Bogoliubov (DHB) model [16] do not match the experimental results at the surface region. Consistent with this fact, theoretical predictions for electron scattering on the ^{16}O nucleus using the DHB charge distribution also do not fit the data [14]. The solid lines in Fig. 10 represent Fermi distributions for the ^{16,18}O nuclei, with radii obtained from Eq. 5. The diffuseness found for the ^{16}O nucleus ($a_N = 0.55$ fm) is significantly smaller than that for the ^{18}O ($a_N = 0.60$ fm). The DHB theoretical calculations indicate that the difference between the ^{18}O and ^{16}O total nucleon densities is mainly due to the corresponding difference between the respective neutron distributions (see Fig. 11). Fig. 12 presents the

contributions to the ^{18}O neutron density of different DHB wave-function components. The results for the ^{16}O nucleus are very similar to those for the ^{18}O, but without the d5/2$^+$ component. We have found experimental values for the d5/2$^+$ component by considering the difference between the total ^{16,18}O nucleon densities at the sensitivity radii. In such a subtraction, we have assumed that the Fermi distribution with $a_N = 0.55$ fm (see Fig. 10) is representative of the experimental ^{16}O density. The experimental results for the d5/2$^+$ component present a similar slope but larger density values in comparison with the theoretical DHB prediction (see Fig. 12). An analysis of the single-particle levels of the theoretical calculations shows, as one might expect, that the falloff of the density in the surface region is roughly determined by the least bound levels. The NL3 potential parameters [17,18] that have been used in the Dirac-Hartree-Bogoliubov calculations [16] were adjusted to reproduce binding energies and charge and neutron radii across the periodic table. It did not take into account single-particle properties, which suggest a direction for future improvements in such a parameter set.

6. Conclusion

In this work, we have presented quasi-elastic and reaction channel data at sub-barrier energies for systems involving the ^{18}O as projectile and we have extended our study to other data sets earlier obtained for systems with the ^{16}O nucleus. In our optical model quasi-elastic data analysis, the imaginary part of the potential is based only on very fundamental grounds: the lack of extra surface absorption. A nonlocal model is assumed to describe the real part of the interaction, which at sub-barrier energies can be associated directly with the folding potential. The energy-dependence of the sensitivity radius has permitted the determination of the nuclear potential over a large range of distances around the barrier radius. The experimental diffuseness value found for the potentials of systems with ^{18}O is significantly larger than that for the ^{16}O nucleus. Within this context, a significant difference between the diffuseness for the densities of the ^{16,18}O nuclei is expected.

If the target densities are known, the density of the projectile can be extracted from a data analysis in a more direct procedure. In these cases, the results for the ^{16,18}O nuclear densities are consistently independent of the target nucleus. The extracted value for the diffuseness of the ^{18}O nucleus is significantly larger than that for ^{16}O. The corresponding difference gives information about the contribution of the two ^{18}O extra neutrons, in particular that in the d5/2$^+$ level.

This work was partially supported by Financiadora de Estudos e Projetos (FINEP), Fundação de Amparo à Pesquisa do Estado de São Paulo (FAPESP), and Conselho Nacional de Desenvolvimento Científico e Tecnológico (CNPq).

---

[1] L. C. Chamon, D. Pereira, E. S. Rossi Jr., C. P. Silva, R. Lichtenthaler Filho and L. C. Gomes, Nucl. Phys. **A582** (1995) 305 .

[2] L. C. Chamon, D. Pereira, E. S. Rossi Jr., C. P. Silva, H. Dias, L. Losano and C. A. P. Ceneviva, Nucl. Phys. **A597** (1996) 253 .

[3] M. A. G. Alvarez, L. C. Chamon, D. Pereira, E. S. Rossi Jr., C. P. Silva, L. R. Gasques, H. Dias and M. O. Roos, Nucl. Phys. **A656** (1999) 187.

[4] C. P. Silva, M. A. G. Alvarez, L. C. Chamon, D. Pereira, M. N. Rao, E. S. Rossi Jr., L. R. Gasques, M. A. E. Santo, R. M. Anjos, J. Lubian, P. R. S. Gomes, C. Muri, B. V. Carlson, S. Kailas, A. Chatterjee, P. Singh, A. Shivastava, K. Mahata and S. Santra, Nucl. Phys. **A679** (2001) 287.

[5] L. C. Chamon, B. V. Carlson, L. R. Gasques, D. Pereira, C. De Conti, M. A. G. Alvarez, M. S. Hussein, M. A. Candido Ribeiro, E. S. Rossi Jr. and C. P. Silva, submitted to Phys. Rev. **C**.

[6] M. A. C. Ribeiro, L. C. Chamon, D. Pereira, M. S. Hussein and D. Galetti, Phys. Rev. Lett. **78** (1997) 3270.

[7] L. C. Chamon, D. Pereira, M. S. Hussein M. A. C. Ribeiro and D. Galetti, Phys. Rev. Lett. **79** (1997) 5218.

[8] L. C. Chamon, D. Pereira and M. S. Hussein, Phys. Rev. **C58** (1998) 576.

[9] I. J. Thompson, Comput. Phys. Rep. **7** (1988) 167.

[10] S. Raman, C. H. Malarkey, W. T. Milner, C. W. Nestor Jr. and P. H. Stelson, At. Data Nucl. Data Tables **36**, 1 (1987).

[11] E. S. Rossi Jr., PhD thesis, Universidade de São Paulo, Brazil (2001).

[12] M. E. Brandan and G. R. Satchler, Phys. Rep. **285** (1992) 142, and references therein.

[13] R. M. Devries and M. R. Clover, Nucl. Phys. **A243** (1975) 528.

[14] M. A. G. Alvarez, E. S. Rossi Jr., C. P. Silva, L. R. Gasques, L. C. Chamon, D. Pereira, M. N. Rao, B. V. Carlson, C. De Conti, R. M. Anjos, P. R. S. Gomes, J. Lubian, S. Kailas, A. Chatterjee and P. Singh, Phys. Rev. **C65** (2002) 014602.

[15] L. R. Gasques, L. C. Chamon, C. P. Silva, D. Pereira, M. A. G. Alvarez, E. S. Rossi Jr., V. P. Likhachev, B. V. Carlson and C. De Conti, to appear in Phys. Rev. **C**.
[16] B. V. Carlson and D. Hirata, Phys. Rev. **C62** (2000) 054310.
[17] G. A. Lalazissis, J. Konig and P. Ring, Phys. Rev. **C55** (1997) 540.
[18] Z. Patyk, A. Baran, J. F. Berger, J. Decharge, J. Dobaczewski, P. Ring and A. Sobiczewski, Phys. Rev. **C59** (1999) 704.

Table 1: The inelastic, one- and two-neutron transfer channels considered in the coupled-channel calculations for the $^{18}O + ^{58}Ni$ system. The excitation energy is quoted in MeV.

^{18}O	^{58}Ni	^{17}O	^{59}Ni	^{16}O	^{60}Ni
$0^+(g.s.)$	$0^+(g.s.)$	$\frac{5}{2}^+(g.s.)$	$\frac{3}{2}^-(g.s.)$	$0^+(g.s.)$	$0^+(g.s.)$
$0^+(g.s.)$	$2^+(1.45)$	$\frac{5}{2}^+(g.s.)$	$\frac{5}{2}^-(0.34)$	$0^+(g.s.)$	$2^+(1.33)$
$2^+(1.98)$	$0^+(g.s.)$	$\frac{5}{2}^+(g.s.)$	$\frac{1}{2}^-(0.47)$	$0^+(g.s.)$	$2^+(2.16)$
		$\frac{1}{2}^+(0.87)$	$\frac{3}{2}^-(g.s.)$	$0^+(g.s.)$	$0^+(2.28)$
		$\frac{5}{2}^+(g.s.)$	$\frac{9}{2}^-(0.88)$	$0^+(g.s.)$	$4^+(2.51)$
		$\frac{5}{2}^+(g.s.)$	$\frac{5}{2}^-(1.19)$	$0^+(g.s.)$	$4^+(3.12)$
				$0^+(g.s.)$	$2^+(3.12)$
				$0^+(g.s.)$	$2^+(3.27)$
				$0^+(g.s.)$	$2^+(3.38)$
				$0^+(g.s.)$	$0^+(3.53)$
				$0^+(g.s.)$	$4^+(3.67)$
				$0^+(g.s.)$	$2^+(3.87)$
				$0^+(g.s.)$	$2^+(4.01)$
				$0^+(g.s.)$	$2^+(4.08)$
				$0^+(g.s.)$	$2^+(4.32)$
				$0^+(g.s.)$	$2^+(4.50)$
				$0^+(g.s.)$	$2^+(4.55)$
				$0^+(g.s.)$	$4^+(5.02)$
				$0^+(g.s.)$	$4^+(5.11)$
				$0^+(g.s.)$	$4^+(5.24)$
				$0^+(g.s.)$	$2^+(5.43)$
				$0^+(g.s.)$	$0^+(5.53)$
				$0^+(g.s.)$	$2^+(5.58)$
				$0^+(6.05)$	$0^+(g.s.)$
				$3^-(6.13)$	$0^+(g.s.)$

Table 2: The inelastic and two-neutron transfer channels considered in the coupled-channel calculations for the $^{18}O + {}^{60}Ni$ system. The excitation energy is quoted in MeV.

^{18}O	^{60}Ni	^{16}O	^{62}Ni
$0^+(g.s.)$	$0^+(g.s.)$	$0^+(g.s.)$	$0^+(g.s.)$
$0^+(g.s.)$	$2^+(1.33)$	$0^+(g.s.)$	$2^+(1.17)$
$2^+(1.98)$	$0^+(g.s.)$	$0^+(g.s.)$	$0^+(2.05)$
		$0^+(g.s.)$	$2^+(2.30)$
		$0^+(g.s.)$	$4^+(2.34)$
		$0^+(g.s.)$	$0^+(2.89)$
		$0^+(g.s.)$	$2^+(3.06)$
		$0^+(g.s.)$	$2^+(3.16)$
		$0^+(g.s.)$	$4^+(3.17)$
		$0^+(g.s.)$	$2^+(3.26)$
		$0^+(g.s.)$	$2^+(3.27)$
		$0^+(g.s.)$	$4^+(3.27)$
		$0^+(g.s.)$	$2^+(3.37)$
		$0^+(g.s.)$	$2^+(3.52)$
		$0^+(g.s.)$	$2^+(3.86)$
		$0^+(g.s.)$	$2^+(3.97)$
		$0^+(g.s.)$	$4^+(3.99)$
		$0^+(g.s.)$	$4^+(4.05)$
		$0^+(g.s.)$	$2^+(4.06)$
		$0^+(g.s.)$	$0^+(4.23)$
		$0^+(g.s.)$	$2^+(4.32)$
		$0^+(g.s.)$	$2^+(4.42)$
		$0^+(g.s.)$	$2^+(5.00)$
		$0^+(6.05)$	$0^+(g.s.)$
		$3^-(6.13)$	$0^+(g.s.)$

Table 3: The Coulomb (δ_c) and nuclear (δ_n) deformation lengths, $B(E2)$ and excitation energies for inelastic excitation considered in the coupled-channel calculations.

nucleus	δ_c (fm)	δ_n (fm)	$B(E2)$ (e^2b^2)	E^* (MeV)
^{18}O	1.26	1.26	45.1	1.98
^{58}Ni	0.96	0.90	688	1.45
^{60}Ni	1.10	1.08	931	1.33

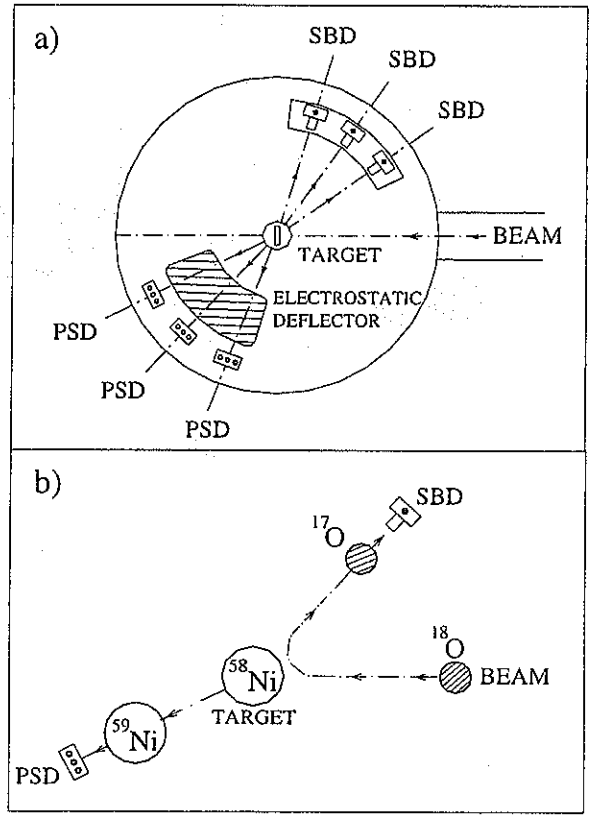

FIG. 1. (a) - The detecting system used in the experiments, with the surface barrier detectors (SBD), position sensitive detectors (PSD) and electrostatic deflector. (b) - Schematic view of the collision for one-neutron transfer, showing the detection of the lighter particle in the SBD and the heavier particle in the PSD.

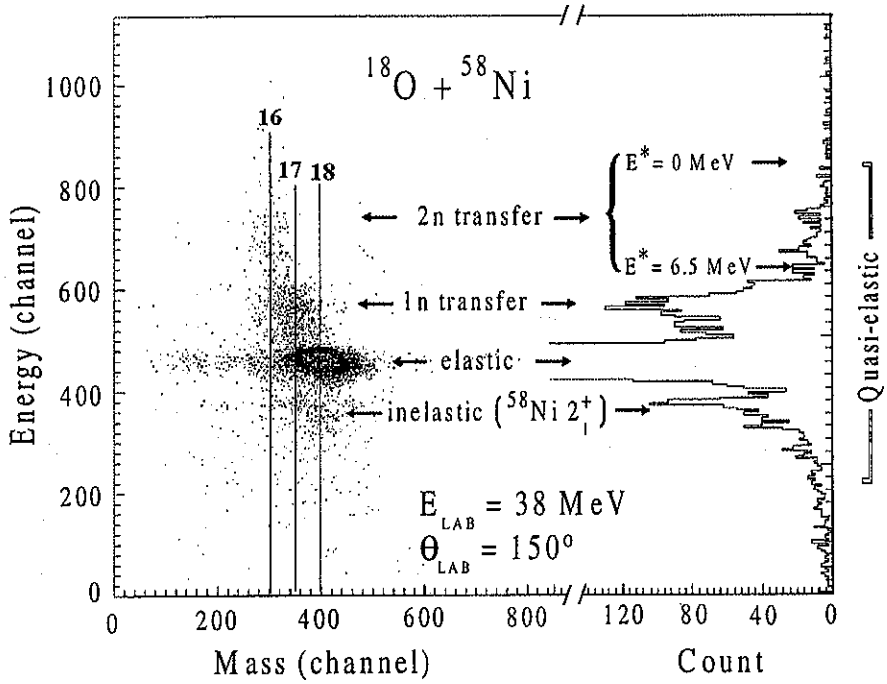

FIG. 2. Typical mass *versus* energy spectrum for the lighter particle and the projection of all events on the energy axis. The mass regions A = 16,17 and 18, and the energy region of relevant channels, including the elastic and quasi-elastic processes, are indicated in the figure.

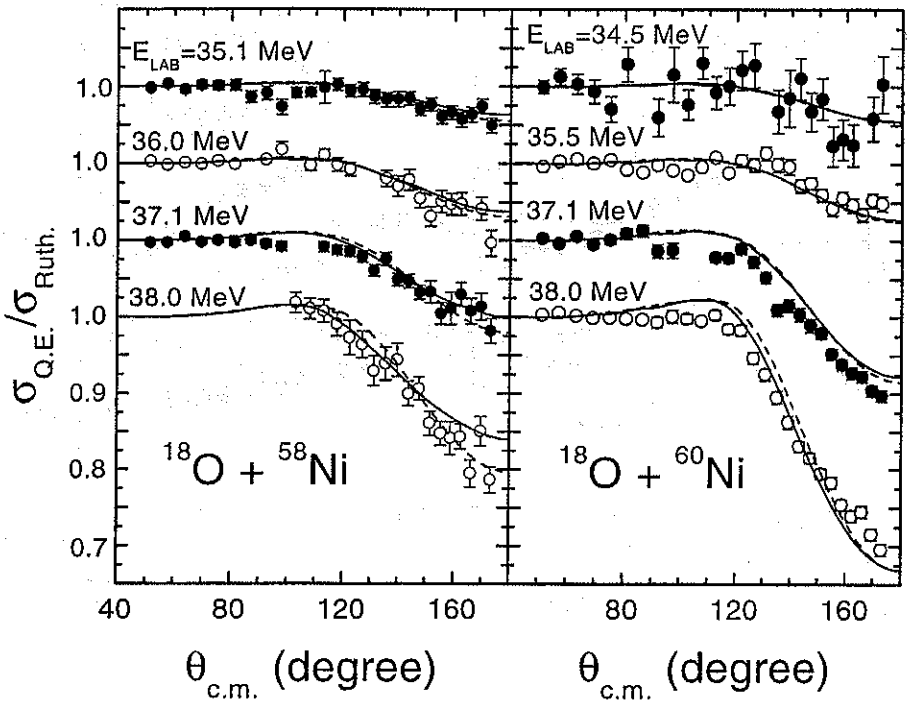

FIG. 3. Quasi-elastic cross sections for the $^{18}O + ^{58,60}Ni$ systems at several sub-barrier energies. The lines represent the results of optical model (dashed lines) and coupled-channel (solid lines) calculations using energy-independent bare potentials.

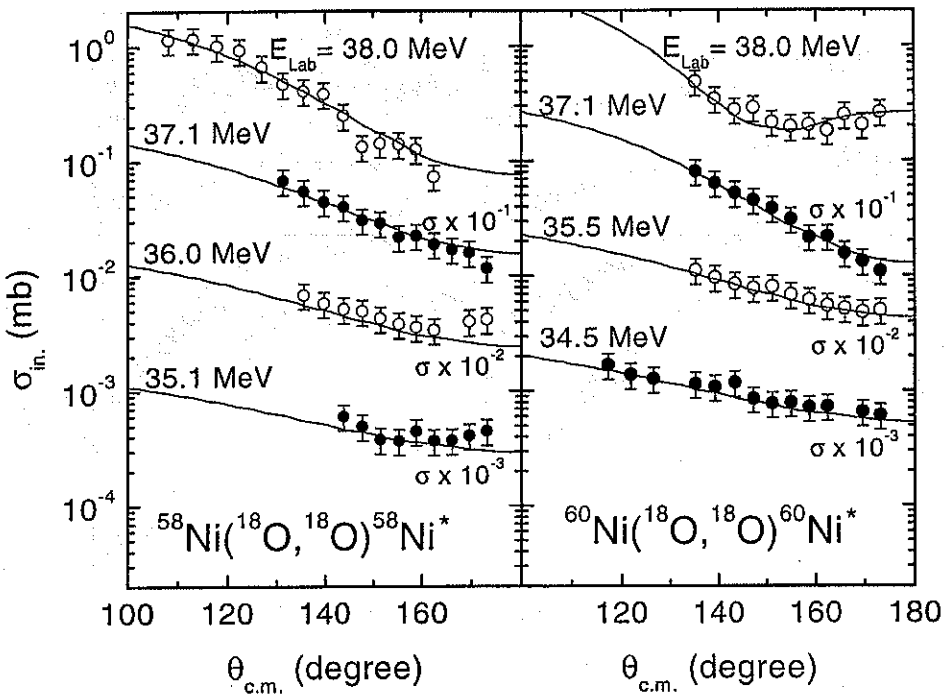

FIG. 4. Inelastic scattering cross sections, with excitation of the 2_1^+ target state, for the $^{18}O + ^{58,60}Ni$ systems at several sub-barrier energies. The lines represent the results of channel-coupled calculations using energy-independent bare potentials.

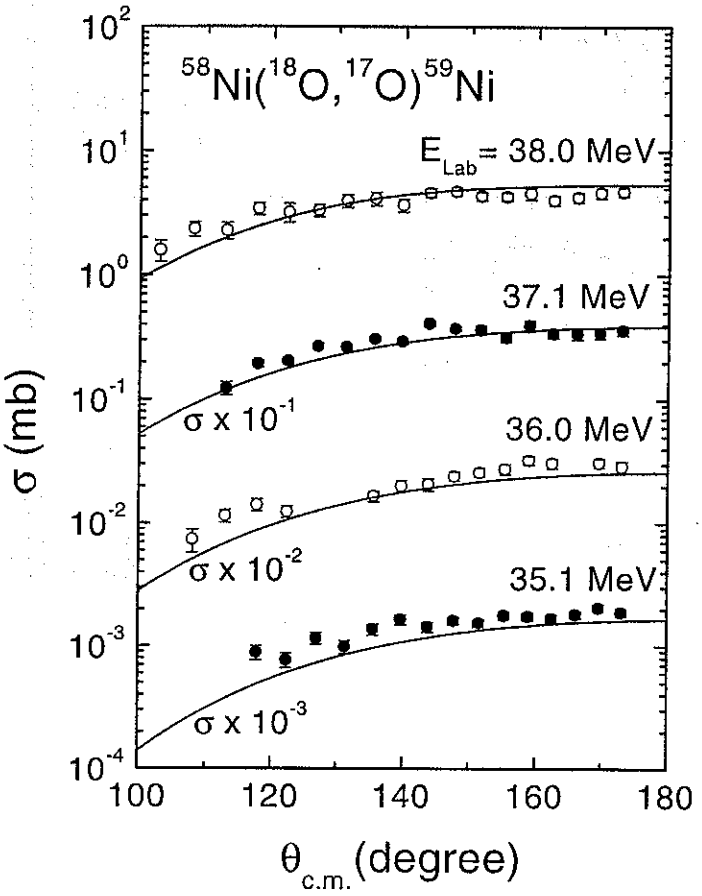

FIG. 5. One-neutron transfer cross sections for the ^{18}O + ^{58}Ni system at several sub-barrier energies. The data include transitions for the ground-state, the first ^{17}O excited state, and four ^{59}Ni excited states. The lines represent the results of channel-coupled calculations using an energy-independent bare potential.

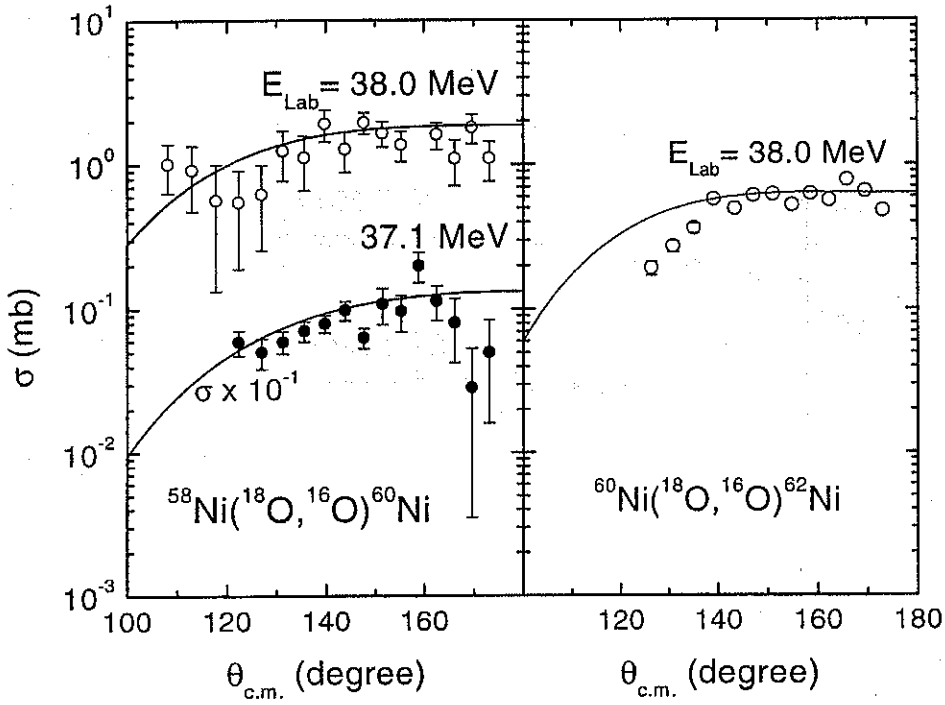

FIG. 6. Two-neutron transfer cross sections for the $^{18}O + ^{58,60}Ni$ systems at sub-barrier energies. The data include transitions to the set of states with excitation energy from 0 to 6.5 MeV (see tables 1 and 2). The lines represent the results of channel-coupled calculations using energy-independent bare potentials.

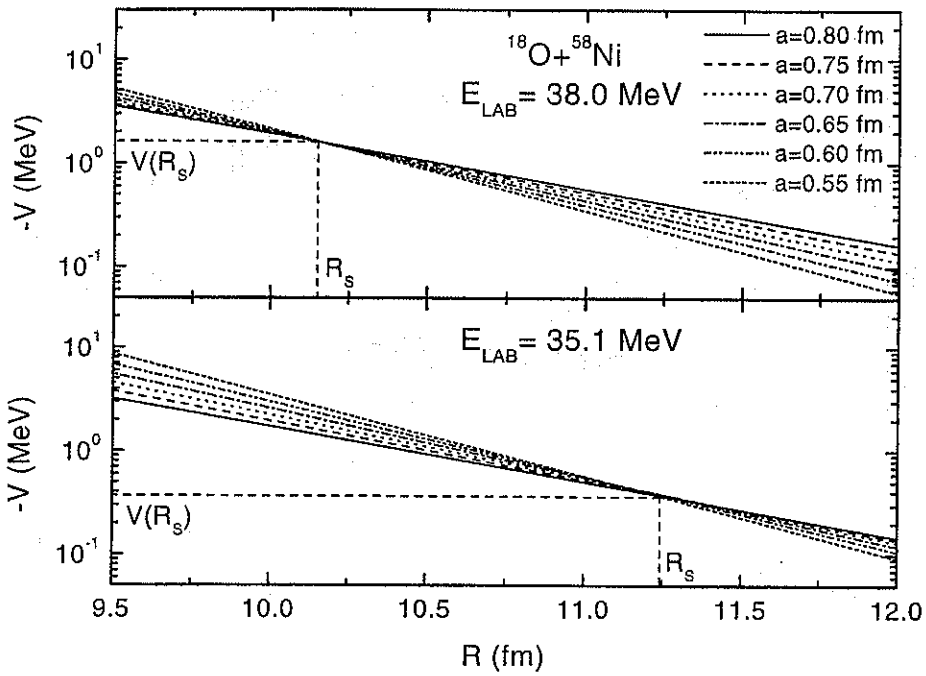

FIG. 7. The real part of the optical potential for the $^{18}O + ^{58}Ni$ system at two different energies, as obtained by optical-model quasi-elastic data fits for several values of the diffuseness parameter. The potentials cross at the sensitivity radius, R_S, where the corresponding potential strength is determined without ambiguity.

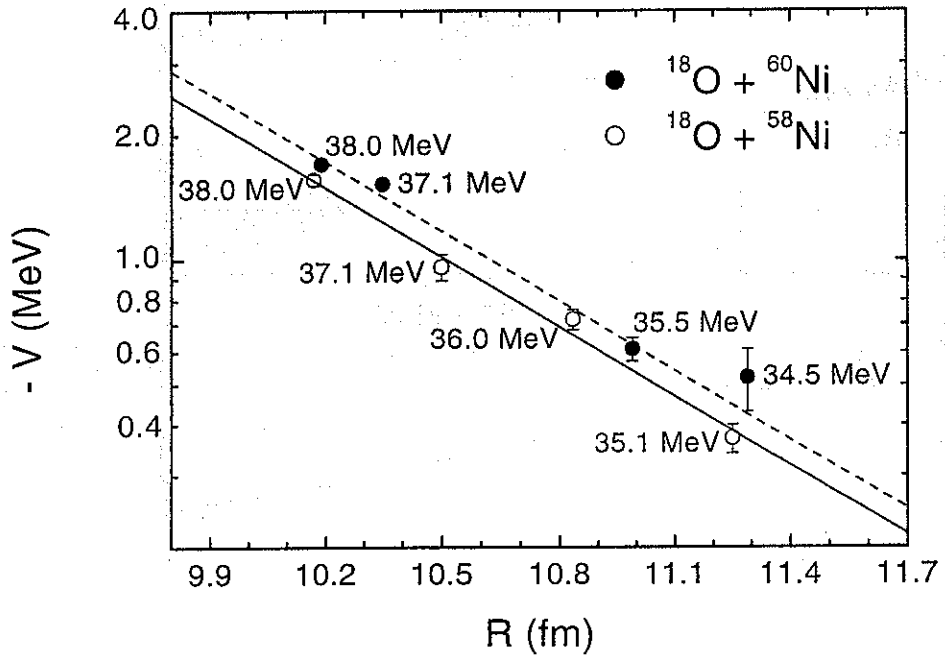

FIG. 8. The nuclear potential strength as a function of the sensitivity radius for the $^{18}O + ^{58,60}Ni$ systems. The bombarding energies of the angular distributions in which the sensitivity radii have been determined are indicated in the figure. The lines represent exponentials with diffuseness 0.77 fm.

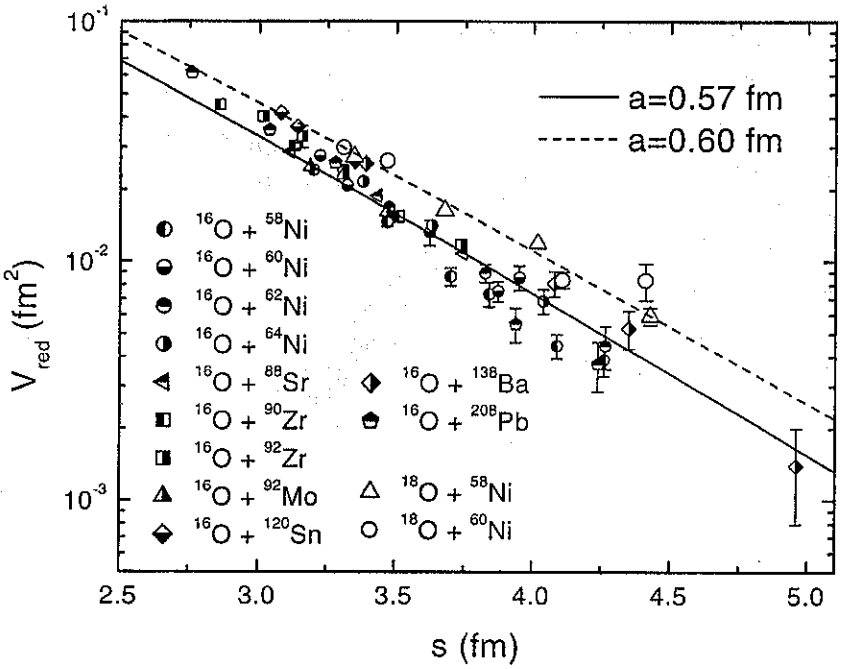

FIG. 9. The experimental reduced potential strength as a function of the reduced distance, s, for several systems involving the ^{16}O (semi-closed symbols) and ^{18}O (open symbols) nuclei as projectiles. The lines represent theoretical predictions, Eq. 11, with different diffuseness values.

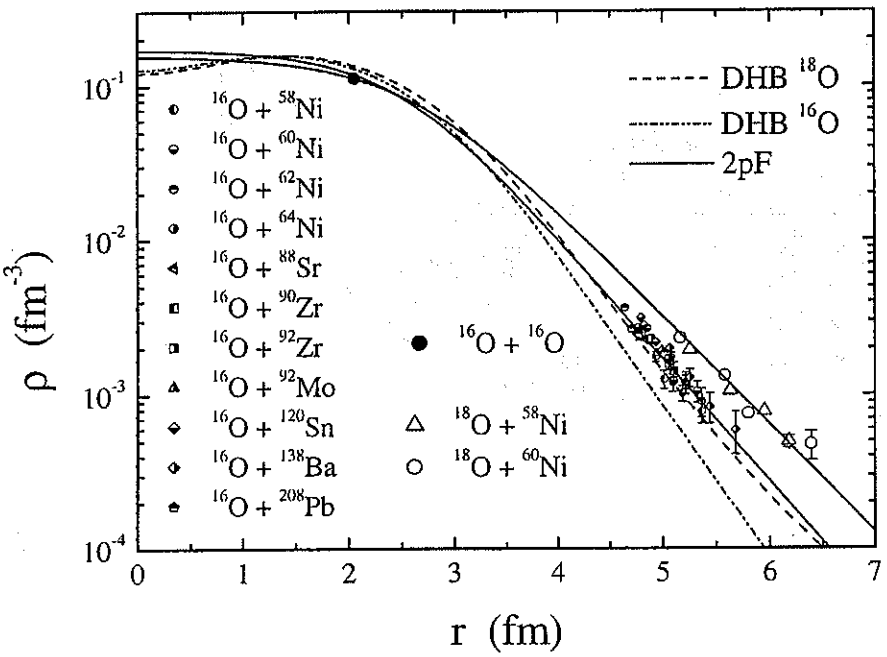

FIG. 10. Experimental nucleon density values for the ^{16}O (semi-closed symbols) and ^{18}O (open symbols) nuclei, as obtained from sub-barrier data analyses for different systems and bombarding energies. The closed symbol represents a density value for the ^{16}O nucleus from intermediate energy data analyses. The lines correspond to theoretical Dirac-Hartree-Bogoliubov (DHB) calculations and two-parameter Fermi (2pF) distributions.

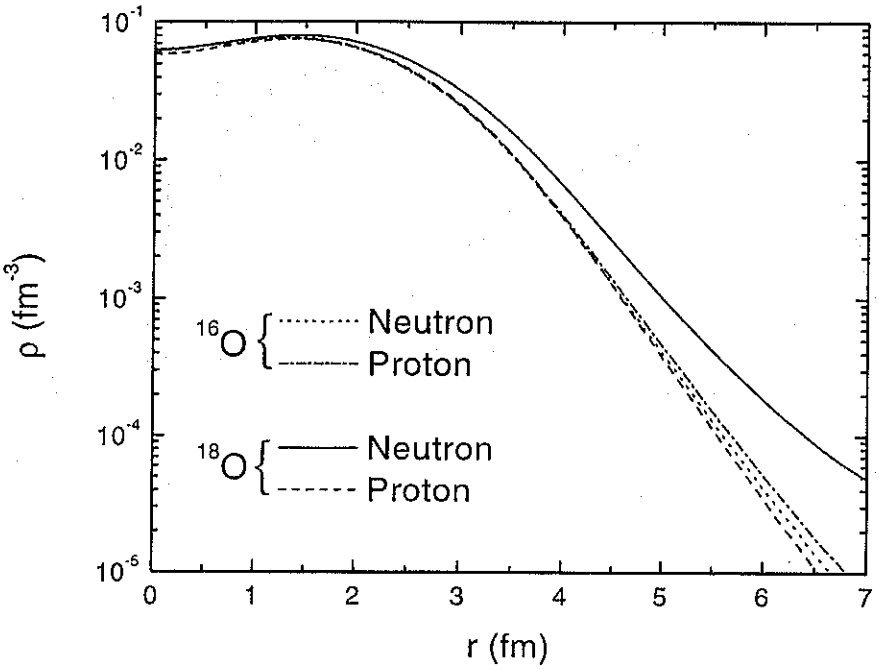

FIG. 11. Comparison among proton and neutron theoretical Dirac-Hartree-Bogoliubov densities for the ^{16,18}O nuclei.

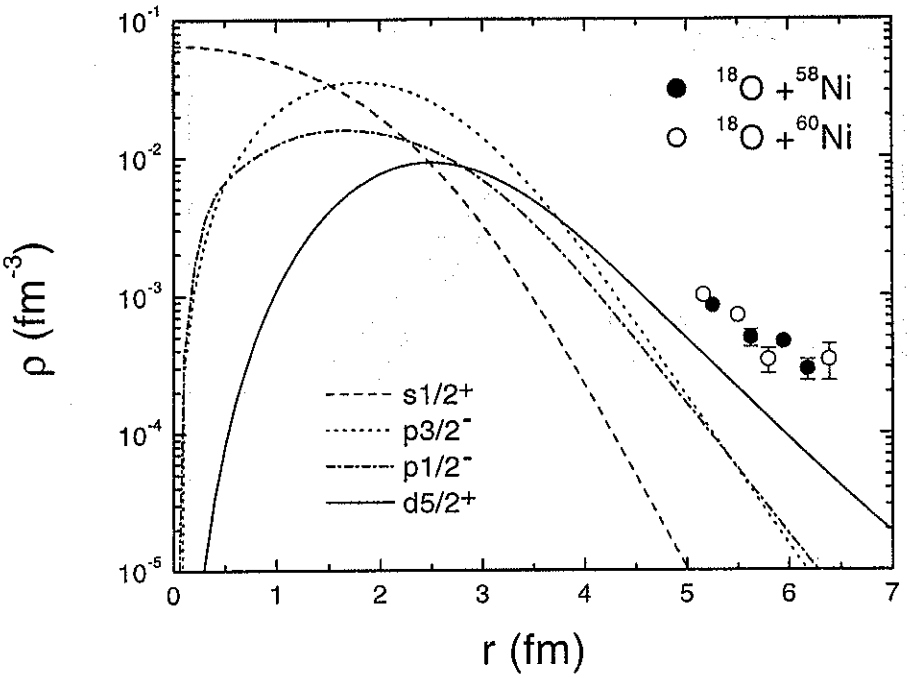

FIG. 12. Theoretical DHB predictions for the ^{18}O neutron density distributed in the main orbitals. The data (open and closed symbols) correspond to the difference between the experimental total nucleon densities for the ^{16,18}O nuclei (see text for details).